Journal of Computer Assisted Tomography
25(3):452–457
© 2001 Lippincott Williams & Wilkins, Inc., Philadelphia

Effects of Image Orientation on the Comparability of Pediatric Brain Volumes Using Three-Dimensional MR Data

Anil J. Patwardhan, Stephan Eliez, Ilana S. Warsofsky, Gary H. Glover, Chris D. White, Jay N. Giedd, Bradley S. Peterson, Donald C. Rojas, and Allan L. Reiss

Purpose: The purpose of this study was to examine the comparability of morphometric measurements made on pediatric data sets collected at five scanner locations, each using variations on a 3D spoiled gradient-recalled echo (SPGR) pulse sequence.

Method: Archived MR data from 60 typically developing children were collected and separated into seven groups based on the pulse sequence used. A highly automated image-processing procedure was used to segment the brain data into white tissue, gray tissue, and CSF compartments and into various neuroanatomic regions of interest.

Results: Volumetric comparisons between groups revealed differences in areas of the temporal and occipital lobes. These differences were observed when comparing data sets with different image orientations and appeared to be due to partial volume averaging (PVA) and susceptibility-induced geometric distortions.

Conclusion: Our results indicate that slice selection and image resolution should be controlled in volumetric studies using aggregated data from multiple centers to minimize the effects of PVA and susceptibility-induced geometric distortions.

Index Terms: Magnetic resonance imaging—Brain—Brain, morphology.

Magnetic resonance imaging (MRI) is now widely used to quantitatively assess the in vivo morphologic properties of the brain, both in the disease state and in normal human brain development. Whereas MRI has proven to be a powerful tool in areas of neuroanatomic research, the pragmatics of large scale longitudinal imaging experiments often require the aggregation of MR scan data from different centers. For example, in studies of disease progression (e.g., multiple sclerosis), there may be a need to acquire scans serially for individual patients over the course of several years. Additionally, in studies requiring a large number of participants, it is often impractical to scan all prospective subjects at a single MR location. Thus, knowledge of the comparability of MR data from different sources is critical. Image compatibility allows for pooling of MR scan data from multiple scan sites, thereby increasing sample size and statistical power, and may permit the collection and use of previously inaccessible or rare data.

Factors that may affect scan compatibility include differences in pulse sequence, image artifacts, scanner hardware and software, and scanner maintenance. To aggregate data from multiple sites, investigators must have knowledge of how differences in these parameters influence the results of their image analysis procedures. In this multicenter study, we used a reliable, well-validated, and largely automated image analysis procedure to examine variability in volume measurements made on scans of children acquired at several research institutions across the country. These data are timely given the recent initiatives to aggregate data from multiple sites in an initial attempt to analyze brain growth and maturation during childhood.

METHODS

Subjects

Archived MR data were obtained from five different research institutions within the United States. Each of the

From the Stanford Psychiatry Neuroimaging Laboratory, Department of Psychiatry and Behavioral Sciences (A. J. Patwardhan, S. Eliez, I. S. Warsofsky, C. D. White, and A. L. Reiss), and Department of Radiology (G. H. Glover), Stanford University School of Medicine, Stanford, CA, Child Psychiatry Branch, National Institute of Mental Health, Bethesda, MD (J. N. Giedd), Yale Child Study Center, Yale University School of Medicine, New Haven, CT (B. S. Peterson), and Department of Psychiatry, University of Colorado Health Sciences Center, Denver, CO (D. C. Rojas), U.S.A. Address correspondence and reprint requests to Dr. A. L. Reiss at Department of Psychiatry and Behavioral Sciences, Stanford University School of Medicine, 401 Quarry Rd., Stanford, CA 94305-5719, U.S.A. E-mail: reiss@stanford.edu

sites contributed scans of five boys and five girls who were individually matched for gender and within 2 years of age among groups. An additional group of 10 subjects was also scanned at one of the sites, for a total of 60 subjects. The 60 subjects in the study were separated into seven groups based on the differences in pulse sequence used among the scanners (see Table 1).

MR Protocols

All data were acquired with 1.5 T GE Signa scanners (General Electric Medical Systems, Milwaukee, WI, U.S.A.). The scanning protocols used for all data acquisitions and analyses included variations on a standard T1-weighted 3D spoiled gradient-recalled echo (SPGR) pulse sequence and varied with scan site as shown in Table 1. The National Institute of Mental Health (NIMH) (Group I), Stanford University (Group IV), and University of Colorado (Group VII) sites each contributed scans from only one group of 10 subjects. Groups V and VI consist of coronal and sagittal acquisitions from the same group of 10 subjects who were scanned twice at the Yale University School of Medicine. Groups II and III consist of coronal acquisitions from two separate groups of 10 subjects, both scanned at Johns Hopkins University School of Medicine.

Raw GE Signa formatted image data were collected, processed, and analyzed in the Stanford Psychiatry Neuroimaging Laboratory (Stanford University School of Medicine, Stanford, CA, U.S.A.) for volumetric analysis. Volumetric measurements were performed using the image analysis program BrainImage (1).

Data Processing

Volumetric assessment of image data in BrainImage requires a stepwise process of data importation, removal of nonbrain voxels, correction of image nonuniformity resulting from RF field inhomogeneity, positional normalization of image data sets, and fuzzy tissue segmentation. Each of these steps has been delineated in previous publications (2–6) and is briefly described here.

The data importation process creates a stack of spatially registered 8 bit images and minimizes the amount of interslice gradient or "shading" artifact due to the RF field inhomogeneity during a scan. For measurements of brain volumes, nonbrain material is removed from the raw data using a semiautomated erosion-dilation, edge detection protocol followed by manual rater adjustments (2). The resulting image stack comprises cranial tissue and CSF only and is devoid of skull, scalp, and vasculature. A correction algorithm is then applied to the resulting brain tissue to again minimize the amount of interslice and intraslice gradient artifact. This "skull-stripped" and corrected image is then resliced to produce an isotropic dataset so that the interpolated slice thickness in the plane of acquisition (z-dimension) has the same resolution as in the x- and y-pixel dimensions.

A multistep tissue segmentation procedure in BrainImage is used for volumetric quantification of whole-brain tissue into white, gray, and CSF tissue compartments and relies on a "fuzzy" or probabilistic classification of voxels based on voxel intensity (3). The segmentation method produces three image stacks, each containing voxels assigned to white tissue, gray tissue, and CSF, respectively.

A method initially described by Andreasen et al. (6) and subsequently modified (4,5) is used to subdivide the brain into cerebral lobes. All resliced brain images are brought into a multiplanar viewing module of BrainImage to standardize their position in space with reference to anterior commissure (AC)-posterior commissure (PC) landmarks. Once the AC–PC plane is set, the BrainImage software automatically loads a proportional stereotaxic grid onto the brain. The grid is composed of 1,232 3D rectangular sectors (6,7) that are grouped together to correspond to neuroanatomic regions of interest (4,5). Volumes of the total cerebrum, frontal

TABLE 1. *Scan parameters for Groups I–VII*

Group	Age at scan (yrs)	TR (ms)	TE (ms)	Flip angle (°)	NEX	Matrix	FOV (mm)	Resolution (x, y, z) (mm)	Orientation
I: Child Psychiatry Branch, NIMH	Mean = 9.80, SD = 2.6	24	5	45	1	256 × 192	240	0.94 × 0.94 × 1.50	Axial
II: Johns Hopkins Univ. School of Medicine	Mean = 10.28, SD = 2.4	45	5, 6	45	1	256 × 128	240, 220	0.94 × 0.94 × 1.50 0.86 × 0.86 × 1.50	Coronal
III: Johns Hopkins Univ. School of Medicine	Mean = 10.53, SD = 2.9	45	5, 6	45	1	256 × 128	240, 200	0.94 × 0.94 × 1.50 0.78 × 0.78 × 1.50	Coronal
IV: Stanford Univ. School of Medicine	Mean = 10.53, SD = 2.4	45	5, 6	45	1	256 × 128	240, 220	0.94 × 0.94 × 1.50 0.86 × 0.86 × 1.50	Coronal
V: Yale Child Study Center, Yale School of Medicine	Mean = 9.50, SD = 2.4	24	8	45	0.75	256 × 192	360	1.41 × 1.41 × 1.40	Coronal
VI: Yale Child Study Center, Yale School of Medicine	Mean = 9.50, SD = 2.4	24	5	45	2	256 × 192	300	1.17 × 1.17 × 1.20	Sagittal
VII: Department of Psychiatry, Univ. of Colorado Health Sciences Center	Mean = 10.24, SD = 2.5	45	5	45	1	256 × 128	240	0.94 × 0.94 × 1.70	Coronal

TABLE 2. *Segmented volumes [mean (SD)] among Groups I–VII and results from seven-group repeated measures ANOVA comparison*

	I	II	III	IV	V	VI	VII	Repeated measures ANOVA
Gray matter								
Cerebrum	711.1 (61.50)	691.0 (64.70)	666.8 (84.94)	687.6 (38.71)	641.7 (57.06)	628.1 (61.23)	652.9 (75.50)	$F = 3.025$, $p \leq 0.0127$
Frontal	251.6 (24.83)	251.4 (23.42)	235.4 (29.24)	248.1 (19.96)	233.0 (21.30)	228.3 (19.30)	236.6 (29.01)	$F = 1.890$, $p \leq 0.0993$
Parietal	171.8 (17.54)	163.9 (13.37)	161.9 (25.07)	162.1 (14.31)	155.5 (14.30)	153.8 (14.74)	159.2 (17.00)	$F = 1.347$, $p \leq 0.2528$
Temporal	155.1 (14.56)	154.5 (22.36)	149.4 (19.35)	158.3 (12.11)	142.7 (16.09)	128.0 (15.63)	143.0 (16.66)	$F = 6.291$, $p < 0.0001$
Occipital	87.1 (9.48)	75.0 (12.15)	74.3 (13.85)	73.9 (8.95)	64.6 (9.75)	73.6 (12.26)	72.7 (14.73)	$F = 4.403$, $p \leq 0.0011$
Vent. CSF	9.2 (4.54)	9.7 (2.47)	8.6 (1.92)	12.2 (6.71)	10.1 (4.21)	10.2 (3.53)	11.2 (4.64)	$F = 0.726$, $p \leq 0.6304$
White matter								
Cerebrum	445.7 (57.57)	454.6 (71.11)	432.2 (79.30)	446.3 (57.10)	427.1 (59.86)	403.5 (44.50)	454.9 (54.94)	$F = 1.413$, $p \leq 0.2265$
Frontal	153.9 (22.27)	169.7 (28.30)	155.8 (30.44)	161.2 (19.31)	154.8 (22.21)	142.7 (16.31)	165.9 (22.84)	$F = 2.289$, $p \leq 0.0485$
Parietal	119.4 (14.79)	116.0 (14.17)	116.6 (20.60)	120.1 (17.29)	112.6 (17.30)	108.0 (15.55)	119.5 (14.49)	$F = 0.855$, $p \leq 0.5336$
Temporal	72.1 (14.01)	68.0 (13.06)	65.2 (13.45)	64.7 (16.09)	66.6 (11.62)	67.0 (7.84)	68.6 (10.78)	$F = 0.632$, $p \leq 0.7040$
Occipital	54.2 (7.85)	53.9 (13.52)	50.1 (14.52)	54.9 (12.81)	51.6 (9.90)	44.7 (7.74)	53.2 (8.82)	$F = 1.308$, $p \leq 0.2697$

lobe, parietal lobe, temporal lobe, occipital lobe, and ventricular CSF were measured using this method.

Statistics

Differences in regional brain volumes among the multicenter groups were computed with repeated measures analysis of variance (ANOVA). If the overall analytic model indicated significant group differences were present, follow-up between-group post hoc analyses were carried out using the Fisher protected least-square difference. The significance threshold for all analyses was $p < 0.01$.

RESULTS

Interrater Reliability

Interrater reliability among three raters was calculated for six brains chosen at random from the multicenter study. The reliability sample consisted of four girls and two boys (age range 9–14 years). Each of the three raters completed each phase of image processing independently for all six brains, and the resulting volumetric data were compared.

The intraclass correlation coefficient was used to calculate interrater reliabilities for segmented areas of brain tissue among three raters. The average intraclass correlation was 0.95, indicating high reliability.

Groupwise Comparison

Total brain volumes were distributed normally among the various groups. ANOVAs revealed no significant difference between groups for age at MR scan ($F = 0.307$, $p < 0.9310$).

Results of the repeated measures ANOVA revealed significant differences in volumes for 3 of the 16 areas assessed: total cerebral gray tissue, temporal lobe gray tissue, and occipital lobe gray tissue (Table 2). Further post hoc analyses specified that Groups I and VI contributed most to these differences (Table 3). Frontal lobe volumes were also reduced in Group VI compared with other groups; however, this difference did not reach significance.

As shown in Table 3, total cerebrum gray volumes were increased in Group I compared with Groups V and VI and were reduced in Group VI compared with Group II. Temporal gray tissue also was reduced in Group VI compared with Groups I, II, III, and IV. Occipital lobe gray volumes were significantly increased in Group I compared with all other groups.

DISCUSSION

Previous studies employing phantoms have examined the accuracy (closeness to truth) and precision (reproducibility) of volumetric measures and spatial localization using multiple sets of MR data. Quantitative MRI-based volumetry (8,9) and stereotactic localization (10)

TABLE 3. *Post hoc analyses (Fisher protected least-square difference) of significant group interactions for regions of interest*

Group interaction	I–II	I–III	I–IV	I–V	I–VI	I–VII	II–VI	III–VI	IV–VI
Cerebrum gray I > V, VI; VI < II				$p \leq 0.0057$, MD = 69.5	$p \leq 0.0011$, MD = 83.0		$p \leq 0.0118$, MD = 62.9		
Temporal gray VI < I, II, III, IV					$p < 0.0001$, MD = 27.1		$p < 0.0001$, MD = 26.5	$p \leq 0.0006$, MD = 21.4	$p < 0.0001$, MD = 30.3
Occipital gray I > II, III, IV, V, VI, VII	$p \leq 0.0090$, MD = 12.0	$p \leq 0.0057$, MD = 12.8	$p \leq 0.0046$, MD = 13.1	$p < 0.0001$, MD = 22.4	$p \leq 0.0037$, MD = 13.5	$p \leq 0.0021$, MD = 14.3			

Significant group interactions for volume differences are listed under particular brain regions in the leftmost column (i.e., I > V, VI). No regions of the frontal lobe, parietal lobe, or ventricles were significantly different in the seven group ANOVA comparison and therefore were not further explored for group interactions. MD, mean difference.

of phantom materials and formalin-fixed brains (11) have shown variations in repeated measures resulting from changes in image orientation and slice thickness, although differences with 3D acquisitions are generally less significant than with 2D data acquisition (8,10). However, without multiple tissue/tissue interfaces and the geometric distortions introduced by the presence of biologic materials in the magnetic field (12), phantoms are often poor representations of clinical MR data. Filippi et al. (11) have previously demonstrated variations in lesion volumes due to differences in field strength and scanner type in a group of adult patients with multiple sclerosis scanned with a 2D dual echo sequence using 5 mm slice thickness. To date, no studies have addressed the extent to which variations in scanner or high resolution 3D pulse sequence affect the comparison of whole-brain volumetric data from typically developing children.

Several potential sources of image variation were addressed in this study in an effort to increase image compatibility among datasets and sites. First, with use of both real and synthetic phantom data sets, a previous evaluation (3) revealed both high reliability and accuracy for the segmentation algorithm used in this study, indicating that variations associated with data processing and analysis contributed minimally to variation in results among groups. Second, the scanner type among all centers was standardized to reduce the effects of hardware and field strength, factors known to produce variations in image quality (11). Third, the use of a 3D volumetric acquisition, in which the entire imaged volume is excited at once with only weak slab selection (12), gives better contiguous slice profiles, producing less cross-talk between slices (13). Studies have shown that increasing slice thickness over 2 mm has a demonstrable effect on the volume data of relatively small structures of the brain such as the amygdala and hippocampus (14) and multiple sclerosis lesions (15), even with 3D acquisitions. Thus, the requirement of relatively thin slice thickness was selected among all centers for the 3D acquisitions to minimize the effects of partial volume averaging (PVA) (8,11,14). Finally, subjects in all groups also were individually age and gender matched to minimize any biologic variation of tissue volumes among groups due to gender or differing stages of neurodevelopment.

Post hoc analysis of individual group-by-group interactions revealed that significant differences in regional volume measures occurred only among comparisons involving Group I (axial orientation) and Group VI (sagittal orientations). Compared with coronally acquired scans, occipital lobe volumes were increased in images with axial orientations, whereas temporal lobe volumes were reduced in images with sagittal orientations (Fig. 1). These differences were apparent only in gray matter tissue. Our results support previously reported variations (16,17) in measures of gray matter structures due to slice orientation in which a slice thickness of 1.4 mm was used (17). The orientation of slice selection on the reformation of 2D data from the 3D volume may exert its influence on morphometric measurements through the effects of

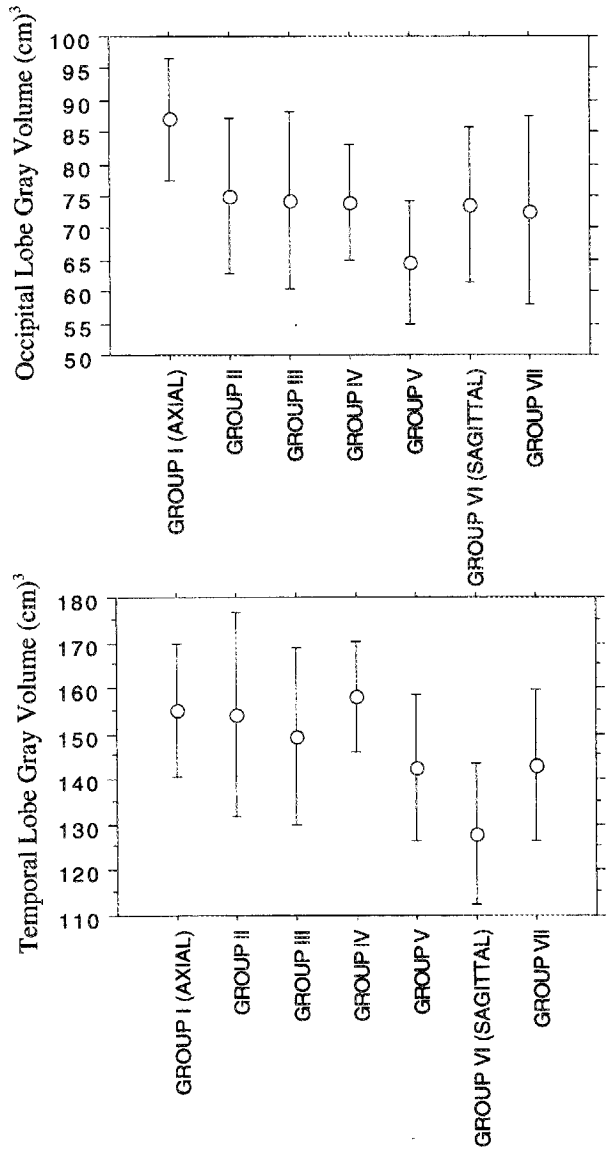

FIG. 1. Seven-group comparison of occipital lobe gray and temporal lobe gray volumes. All groups consisted of coronally oriented images except for Groups I (axial) and VI (sagittal).

PVA (8) in the plane of slice selection. Susceptibility-induced geometric distortions, occurring in the frequency-encoding but not phase-encoding direction (12,18), also may have contributed to volume differences in Group VI in areas of the temporal lobe and frontal lobe.

The amount of PVA occurring among scans depends on essentially three pulse sequence parameters that determine the final resolution in each of the three image dimensions. Field of view, slice thickness, and acquisition matrix size all may affect volume measurements by preferentially affecting any single image plane. When the frequency- and phase-encoding steps are equal and the in-plane resolution equals the resolution in the direction of slice selection, isotropic or "cubic" voxel data are acquired. By acquiring cubic voxels, an equal resolution

in all three image dimensions is ensured, thus avoiding degradation during image reformation due to the large voxel size (13) and eliminating the need for volume reslicing of the reformed 2D image data.

In all of the groups, the number of phase-encoding steps in one of the image planes was reduced to lessen scan time, giving nonsquare acquisition matrix sizes (i.e., 256 × 192). The trade-off is the preferential loss of image resolution in one direction perpendicular to the plane of slice selection due to image reformation into a 256 × 256 final matrix size. Thus, volumetric differences observed in this study may occur as a result of the different acquisition matrix sizes used in these groups. For Groups I and VI, the 256 × 192 matrix size will produce less of a loss of resolution in the phase-encoding direction than in Groups II, III, and VII, which have an acquisition matrix size of 256 × 128. A loss in image resolution in combination with differences in the image orientation may combine to cause the volume differences observed in this study.

Although all groups used relatively thin slice thickness, Groups V and VI had in-plane resolutions that most closely approximated the resolution in the plane of slice selection. Unlike the other axial and coronal data sets, both the coronal scans of Group V and the sagittal scans of Group VI acquired voxel data using a relatively large field of view and low in-plane resolution. Effects of PVA, although present in these lower resolution scans, do not preferentially affect the slice selection dimension, and therefore the volumetric errors do not occur preferentially in any single image plane. Despite the relatively equal resolutions in both Groups V and VI, relatively minor differences in temporal and frontal lobe gray volumes were seen even between these two groups. These differences are remarkable considering that Groups V and VI are coronal and sagittal scans of the same individuals scanned with the same MR machine and may be associated with susceptibility induced distortions in the images.

Apart from differences in image resolution, image artifacts that depend on (focal) magnetic field inhomogeneities also can affect scan compatibility. Susceptibility-induced geometric and intensity distortions occur as a result of magnetic perturbations induced by the imaged object itself and depend on the shape, orientation, and type of material present in the imaged volume (12) and the direction and strength of the gradient field. In MRI, these distortions occur where objects have boundaries with different magnetic susceptibilities and often are present in gradient-recalled echo sequences using large main magnetic field strengths and small read-out gradient strengths (19). In the head, anatomic structures adjacent to regions between air and soft tissue or cortical bone (e.g., frontal and sphenoid sinuses, temporal lobes) are subject to large susceptibility effects. In the current study, susceptibility artifacts were most evident in the sagittal images of Group VI and occurred in the inferior portions of the temporal lobes and frontal lobes, producing an apparent loss of gray matter tissue (Fig. 2). Notably, similar artifacts were absent in coronal images of the same subjects scanned using the same scanner hardware, software, and head position (Group V). The decrease in temporal lobe gray volumes in Group VI compared with other groups, therefore, cannot be completely explained by object-dependent or machine-dependent variables. Among other factors, susceptibility artifacts

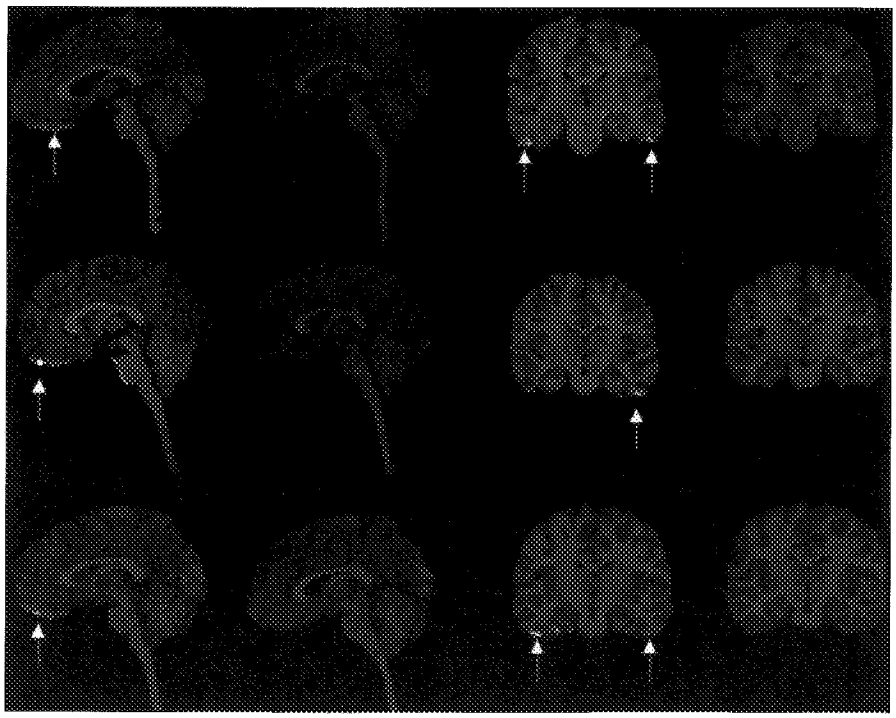

FIG. 2. Susceptibility-induced geometric distortions in 3D acquisitions using both coronal and sagittal slice selections. Shown in the figure is a selection of six subjects who were scanned both coronally (Group V) and sagittally (Group VI). The images were reoriented and resized for visual comparison. Reformatted sagittal sections of the same brain scanned both sagittally (column 1) and coronally (column 2) are shown. Coronal sections of three brains scanned sagittally (column 3) and coronally (column 4) also are presented. Arrows point to the bright intensity variations occurring in the sagittally acquired scans in areas of the temporal lobe and inferior frontal lobe. Note that similar regions in scans acquired in the coronal plane show little or no sign of this artifact.

are dependent on the direction and strength of the magnetic field gradient applied during the scan. In 3D acquisitions, slab selection is relatively weak and is achieved by applying a discrete linear magnetic field gradient (phase-encode gradient) during the period that the broadband, nonselective RF pulse is applied. Differences in the direction of this phase-encoding gradient for sagittal and coronally acquired images may cause orientation-dependent artifacts of the same imaged volume.

Differences in image volumes occurred among scans acquired in different MR centers despite the relatively thin slice thickness used and the increased image quality afforded by 3D acquisitions. Standardizing the direction and thickness of slice selection in 3D acquisitions can minimize the effects of PVA and susceptibility-induced distortions, thereby increasing the compatibility of scans across different sites. Our results indicate that slice selection and image resolution should be carefully controlled in multicenter studies in which aggregation of MR data sets is the primary goal.

Acknowledgment: The authors thank Jennifer Boutin (Stanford Psychiatry Neuroimaging Laboratory) for her help in data processing. This work was supported by NIH grants MH01142 and HD31715.

REFERENCES

1. Reiss A. BrainImage [image analysis program]. Stanford Psychiatry Neuroimaging Laboratory, Stanford, CA, U.S.A., 2000. Available at: http://www-cap.stanford.edu/research/neuroimaging/imageanalysis/getbrainimage.html
2. Subramaniam B, Naidu S, Reiss AL. Neuroanatomy in Rett syndrome: cerebral cortex and posterior fossa. *Neurology* 1997;48:399–407.
3. Reiss AL, Hennessey JG, Rubin M, et al. Reliability and validity of an algorithm for fuzzy tissue segmentation of MRI. *J Comput Assist Tomogr* 1998;22:471–9.
4. Kaplan DM, Liu AM, Abrams MT, et al. Application of an automated parcellation method to the analysis of pediatric brain volumes. *Psychiatry Res* 1997;76:15–27.
5. Kates WR, Warsofsky IS, Patwardhan A, et al. Automated Talairach atlas-based parcellation and measurement of cerebral lobes in children. *Psychiatry Res* 1999;91:11–30.
6. Andreasen NC, Rajarethinam R, Cizadlo T, et al. Automatic atlas-based volume estimation of human brain regions from MR images. *J Comput Assist Tomogr* 1996;20:98–106.
7. Talairach J, Tournoux P. *Co-Planar Stereotaxic Atlas of the Human Brain.* New York: Thieme Medical, 1988.
8. Luft AR, Skalej M, Welte D, et al. Reliability and exactness of MRI-based volumetry: a phantom study. *J Magn Res Imag* 1996;6:700–4.
9. Rusinek H, Chandra R. Brain tissue volume measurement from magnetic resonance imaging: a phantom study. *Invest Radiol* 1993;28:890–5.
10. Walton L, Hampshire A, Forster DM, et al. Stereotactic localization with magnetic resonance imaging: a phantom study to compare the accuracy obtained using two-dimensional and three-dimensional data acquisitions. *Neurosurgery* 1997;41:131–9.
11. Filippi M, van Waesberghe JH, Horsfield MA, et al. Interscanner variation in brain MRI lesion load measurements in MS: implications for clinical trials. *Neurology* 1997;49:371–7.
12. Sumanaweera TS, Adler JR Jr, Napel S, et al. Characterization of spatial distortion in magnetic resonance imaging and its implications for stereotactic surgery. *Neurosurg* 1994;35:696–704.
13. Bushberg JT, Seibert JA, Leidholdt EM, et al. *The Essential Physics of Medical Imaging.* Baltimore: Williams & Wilkins, 1994.
14. Laakso MP, Juottonen K, Partanen K, et al. MRI volumetry of the hippocampus: the effect of slice thickness on volume formation. *Magn Res Imag* 1997;15:263–5.
15. Molyneux PD, Tubridy N, Parker GJ, et al. The effect of section thickness on MR lesion detection and quantification in multiple sclerosis. *AJNR* 1998;19:1715–20.
16. Hasboun D, Chantome M, Zouaoui A, et al. MR determination of hippocampal volume: comparison of three methods. *AJNR* 1996;17:1091–8.
17. Bartzokis G, Altshuler LL, Greider T, et al. Reliability of medial temporal lobe volume measurements using reformatted 3D images. *Psychiatry Res* 1998;82:11–24.
18. Eckstein F, Stammberger T, Priebsch J, et al. Effect of gradient and section orientation on quantitative analysis of knee joint cartilage. *J Magn Res Imag* 2000;11:161–7.
19. Ludeke KM, Roschmann P, Tischler R. Susceptibility artefacts in NMR imaging. *Magn Res Imag* 1985;3:329–43.